

Derivation of coarse-grained potentials via multistate iterative Boltzmann inversion

Timothy C. Moore and Christopher R. Iacovella
*Department of Chemical and Biomolecular Engineering,
 Vanderbilt University, Nashville, TN 37235 USA and
 Vanderbilt Multiscale Modeling and Simulation (MuMS) Center,
 Vanderbilt University, Nashville, TN 37235 USA*

Clare McCabe*
*Department of Chemical and Biomolecular Engineering,
 Vanderbilt University, Nashville, TN 37235 USA
 Vanderbilt Multiscale Modeling and Simulation (MuMS) Center,
 Vanderbilt University, Nashville, TN 37235 USA and
 Department of Chemistry, Vanderbilt University, Nashville, TN 37235 USA*
 (Dated: March 2, 2022)

In this work, an extension to the standard iterative Boltzmann inversion (IBI) method to derive coarse-grained potentials is proposed. It is shown that the inclusion of target data from multiple states yields a less state-dependent potential, and is thus better suited to simulate systems over a range of thermodynamic states than the standard IBI method. The inclusion of target data from multiple states forces the algorithm to sample regions of potential phase space that match the radial distribution function at multiple state points, thus producing a derived potential that is more representative of the underlying potential interactions. It is shown that the algorithm is able to converge to the true potential for a system where the underlying potential is known. It is also shown that potentials derived via the proposed method better predict the behavior of n -alkane chains than those derived via the standard method. Additionally, through the examination of alkane monolayers, it is shown that the relative weight given to each state in the fitting procedure can impact bulk system properties, allowing the potentials to be further tuned in order to match the properties of reference atomistic and/or experimental systems.

I. INTRODUCTION

The utility of coarse-grained (CG) forcefields for soft matter and biological simulations has been well established in the literature, enabling simulation to explore greater length- and time-scales than is feasible with fully atomistic models. This is of particular importance when studying the self-assembly of soft matter systems, where the assembly is typically driven by weak forces, (e.g., hydrophobicity and entropy) [1–6] and structures often demonstrate hierarchical ordering (e.g., molecules organized into micelles, micelles organized into local/global patterns). [5, 7–11] While generic, non-specific CG models have been widely applied, [12–16] providing important information regarding trends and design rules, it is often necessary to use CG models specifically mapped to the system of interest to provide a direct one-to-one correspondence with experiment. While several transferable CG forcefields, such as TraPPE-CG [17] and MARTINI,[18] have been developed, akin to forcefield development at the atomistic level, [19–23] the development of new CG forcefields is still often necessary. This is often required since the available forcefields may be lacking the necessary molecular species/groupings or may not have been optimized for the properties of interest. This second point is of particular consequence, since, for example, a

forcefield optimized to match phase behavior may not appropriately capture subtle structural features.[17] Generally speaking, direct structural correspondence is needed to accurately transition between different simulation levels (e.g., atomistic to CG), in order to perform multiscale [24–26] and hybrid-multiscale simulations, [27–33] as well as to recover atomistic details from CG simulations. [34–37]

Several approaches have been developed to derive and optimize CG forcefields. [38–44] Among these, the iterative Boltzmann inversion (IBI) method[38] has become a popular choice due to its straightforward nature, general applicability to a wide range of systems, and basis in structural properties. The IBI method relies on self-consistently adjusting a given potential to achieve convergence with target structural data; for nonbonded interactions this target data takes the form of the radial distribution function (RDF) between interaction sites and the potential is iteratively updated according to:

$$V_{i+1}(r) = V_i(r) + \alpha k_B T \ln \left[\frac{g^i(r)}{g^*(r)} \right] \quad (1)$$

where $V_i(r)$ is a numerical pair potential; i represents the current iteration; α is a damping factor to suppress large changes to the potential update, often varying from 0.2 to unity, where smaller values tend to be necessary to capture dense and/or crystalline states;[45] k_B is the Boltzmann constant; T the absolute temperature; r the separation between particles; $g_i(r)$ the pair RDF from

* c.mccabe@vanderbilt.edu

the simulation of $V_i(r)$, and $g^*(r)$ the RDF of the target system mapped to the CG level. Although the CG potentials derived from IBI are typically able to accurately reproduce the target RDFs, they are, in general, only applicable at the state point for which they were derived, due to the structural nature of their derivation (e.g., note the explicit temperature dependence of Equation 1, as well as the implicit temperature and density dependence through the $g(r)$ terms).[46, 47] For example, separate potentials were required to capture both the solid and fluid structures of a pure simple lipid;[45] Qian, *et al.*[48] found that the potential derived using IBI for ethylbenzene scales in a non-linear fashion with temperature (i.e., a square root dependence); and several works have shown that CG polymer potentials derived via the IBI method can depend on the chemical environment for which they were derived. [38, 49, 50] Recent work has shown that some of the CG potentials in a benzene-urea-water system derived via IBI have some degree of state point transferability,[51] but it is unclear why IBI provides transferability for some but not all. Furthermore, for complex systems, it may not be possible to optimize the potentials at the state points of interest, due to time- or length-scale limitations of the atomistic simulations and/or system complexity (i.e., systems many unique interactions that need to be derived simultaneously); thus making it difficult to apply the IBI method appropriately, given that potentials are not necessarily transferable. Perhaps of most concern is the fact that the IBI method does not guarantee a unique solution, as a multitude of vastly differing potentials may give rise to otherwise matching RDFs. The form of the final derived potential may also vary based on runtime parameters, such as the initial potential guess, potential cutoff, magnitude of the damping factor, etc. Additionally, the derived potential may include artifacts associated with intermediate and long-range structural correlations in the system, e.g., oscillatory behavior in the potential that follows the peaks and valleys in the RDF, which may alter other properties of the system, even if RDFs match.

In this work, the IBI method is extended to perform multi-state optimization, i.e., the potential is self-consistently adjusted to achieve simultaneous convergence of target data from multiple states. The general idea, illustrated in Figure 1, is that the inclusion of target data from multiple states adds constraints to the optimization problem, such that the derived forcefield tends toward a single potential that can adequately represent all states. For example, potentials in region ‘i’ of the upper portion of Figure 1 are able to match the target structure at a single state ‘i’, potentials in region ‘ii’ are able to reproduce target data at state ‘ii’, etc., with a single representative potential lying at the overlap of these regions, shown as region ‘iv’. To test the efficacy of the proposed multi-state iterative Boltzmann inversion (MS IBI) method, in Section III A, we first perform potential optimizations for the idealized system of a Lennard-Jones (LJ) fluid for which the potential is known, in or-

der to determine if the method resolves the correct potential. In Section III B, to test the method in a system where only nonbonded interactions are present in the CG model, a 3-to-1 mapped CG forcefield is optimized for propane using target data generated from united-atom (UA) propane simulations, and compared with a single-site LJ model mapped to the experimental critical point of propane. In Section III C, we apply this approach to *n*-dodecane, a system more representative of the typical application of a CG forcefield. In Section III D, we examine a monolayer system composed of *n*-dodecane, where it is demonstrated that adjustment of the relative weights given to each target in the MS IBI method can be used to tune the potentials to match other measurable system properties beyond the RDF.

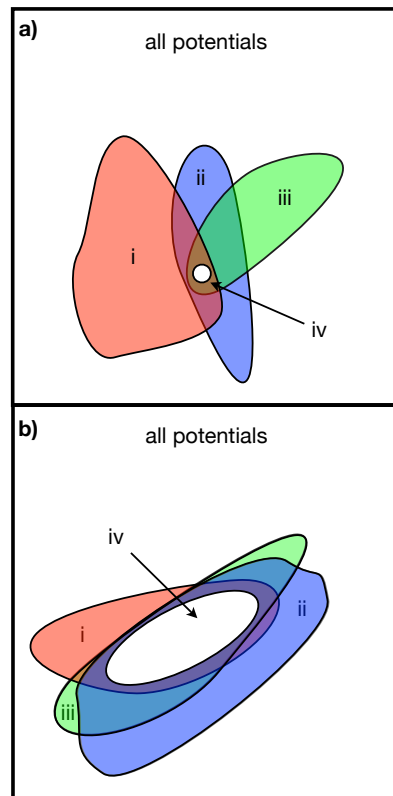


FIG. 1. Regions of good potential phase space for states with optimal overlap (top) and too much overlap (bottom).

II. METHODS AND SIMULATION DETAILS

A. Single-state iterative Boltzmann inversion

In the IBI method (which for clarity we shall refer to as single state, SS IBI), a numerical pair potential, $V(r)$ is iteratively updated according to Equation 1. In this manner, $V(r)$ is updated at each separation, r , based on whether the RDF overpredicts or underpredicts the target RDF at the given r , and is repeated until the trial

RDF matches the target RDF within some tolerance.[38] The initial guess of the numerical potential is often taken to be the Boltzmann inversion of the RDF of the target system:

$$V_0(r) = -k_B T \ln g^*(r) \quad (2)$$

While not exact for site-site interactions in molecules,[52] this methodology is motivated by the statistical mechanics relationship between the potential of mean force (PMF) and the RDF, and provides a reasonable starting potential over which to iterate.

Typically, potentials derived with this method are capable of reproducing the target RDFs with high accuracy, with slight deviations resulting from information lost during coarse-graining. The ease of use of the IBI method and its general applicability make it a powerful tool; given a CG mapping and a target RDF, site-site pair potentials can be readily derived with little user input.

B. Multistate extension of IBI

Although potentials derived with SS IBI will typically reproduce their target RDFs with high accuracy, caution must be taken when using the potentials. Upon successful convergence of the potential, it is only guaranteed that the derived and target RDFs match, not that the potential is necessarily representative of the “true” underlying potential (i.e., not necessarily state independent). It is important to note, especially since information is lost due to coarse-graining, that a multitude of potentials may give rise to similar RDFs. Only a small portion of the potentials that produce matching RDFs may actually fall within the region of potentials that match the true potential and, since the true potential is typically unknown, it is difficult to assess the accuracy of the derived potentials. If the derived potential falls far outside the true potential region, this may give rise to potentials that, despite providing a good match for the target RDF, lack transferability and may contain artifacts making them incapable of resolving system properties other than the RDF.

The proposed MS IBI method aims to minimize the state dependence of the derived potentials by adding additional constraints to the optimization process such that the derived potentials fall within the region of phase space where potentials are representative of the “true” potential. This approach relies on two key assumptions: (1) different thermodynamic states have different regions of the potential phase space that adequately reproduce their respective target RDFs, and (2) that the true, underlying potential lies within the common overlap between these regions of phase space. As the name suggests, this is accomplished by updating the derived potential to simultaneously match target RDFs at different thermodynamic states, producing a single potential that provides sufficient matching for all target RDFs considered. As shown graphically in the upper portion of Figure 1,

the converged potential lies at the intersection of each of the regions representing the target RDFs, as this is the only region where a sufficient match will be found for all states.

The implementation of MS IBI is similar to that of SS IBI, the only additional requirement is more target data. As in SS IBI, the initial potential is assumed to be the Boltzmann inversions of the target RDFs, averaged over the N states used,

$$V_0(r) = -\frac{1}{N} \sum_s k_B T_s g_s^*(r) \quad (3)$$

where the subscript s represents the property at state s . After a trial CG simulation is run at each state using the potential from Equation 3, the potential is updated according to:

$$V_{i+1}(r) = V_i(r) + \frac{1}{N} \sum_s \alpha_s(r) k_B T_s \ln \left[\frac{g_s^i(r)}{g_s^*(r)} \right] \quad (4)$$

While in SS IBI, α represents a damping factor useful for suppressing fluctuations in the potential update, here $\alpha_s(r)$ also serves as a weighting factor, allowing more or less emphasis to be put on each state. For example, if fitting a potential with three states, where state 1 will ultimately be of most interest, it may make sense to give state 1 a higher α value; this will be discussed later in Section III D. Additionally, here $\alpha_s(r)$ is defined as a linear function of the separation r , with the points $\alpha(0) = \alpha_{max}$, and $\alpha(r_{cutoff}) = 0$, such that we ensure the derived potential has a value of zero at the interaction cutoff, r_{cutoff} (i.e., the point at which we assume that pair interactions are zero). Since α decreases as r increases, increased emphasis is placed on shorter-range interactions compared to long-range interactions, similar to the radial dependence of the pressure correction formula often used with IBI.[38] This helps to suppress the influence of long-range structural correlations on the derived potential, as short-range interactions may certainly give rise to long-range correlations (e.g., the formation of bulk crystals from particles interacting through a short-ranged, truncated potential). For direct comparability in this work, both SS and MS IBI treat the damping factor as a linear function of separation, with a fixed value of 0 at the potential cutoff. Note that, although bonded interactions may be optimized in a similar manner (i.e., adjusting the potential to match a target distribution), in this work, we make the assumption that bonded and nonbonded interactions are sufficiently independent such that we use analytical bonded potentials, as has been done in previous work.[45, 53, 54]

The choice of states used in the fitting procedure is naturally important to deriving an accurate potential. To derive the potential most representative of the underlying one, it would not be beneficial to choose states with RDFs that are too similar, as the overlap region would be large, essentially providing minimal additional constraints; this situation is shown in the lower portion

of Figure 1. In such a case, there would be no advantage to the multistate fitting. At the other end of the spectrum, there may in fact be no overlap between states, or more specifically, no overlap for a given level of matching (i.e., no overlap without relaxing the tolerance of an RDF similarity test). For some systems, it may not be possible to define a single pair potential that accurately reproduces the target structure at all states. This is not a problem unique to CG potentials, as it applies at all levels of modeling, e.g., classical atomistic potentials may also lack full state-independence given that they do not allow variation in electron density.

C. Simulation Model

In this work, simulations were performed using 3 distinct models: generic LJ fluid, TraPPE-UA, and CG models derived via IBI. First, simulations of monatomic LJ spheres were performed in the canonical ensemble (i.e., fixed number of particles N , volume V , and temperature T), with temperature controlled via the Nosé-Hoover thermostat. These monatomic LJ systems contained 1468 particles initially randomly distributed throughout the box, and were run for 1×10^6 timesteps, during which the reduced temperature was decreased from 2.0 to the final target temperature. The systems were further equilibrated for 1×10^6 timesteps before target data was collected over 1×10^5 steps. A timestep of 1×10^{-3} reduced time units was used. The interaction parameters used in all LJ simulations were $\sigma = 1.0$ and $\varepsilon = 1.0$, with a potential cutoff $r_{cutoff} = 3\sigma$. Here, no coarse-graining was applied to the target systems, as these simulations were used simply to test the efficacy of the potential derivation under the ideal circumstances where the true potential is known.

The second model used relies on the TraPPE-UA forcefield for simulation.[19] Here, alkanes were simulated in the canonical ensemble, with temperature controlled via the Nosé-Hoover thermostat. Bulk fluid systems for both propane (1024 molecules) and n -dodecane (400 molecules) were simulated at 3 different states, as listed in Section III, and used to generate target RDF data. Although not an all-atom model (as hydrogens are not explicitly modeled), the TraPPE forcefield was chosen for computational convenience, since, in principle, the target data can come from any source. In all cases, a timestep of 1 fs was used. After an initial equilibration period of 5 ns, data was collected over a 10 ns production run. In addition to the bulk fluid n -dodecane simulations, UA simulations were performed of n -dodecane gel and fluid monolayers, composed of 100 n -dodecane chains each. These were performed in the same manner as the bulk simulations at 298 K, but with the first bead of each chain held stationary such that a 2D hexagonally arranged periodic array with density 4.10 chains per nm^2 (gel) and 3.79 chains per nm^2 (fluid) was achieved; these were chosen to match state points commonly used in alkylsilane

monolayer simulations and experiments.[55]

The third model used is a CG representation of alkanes. In all cases a 3-to-1 CG model (i.e., each CG bead represents 3 UA carbon groups) was used to simulate bulk fluid and monolayer systems of alkanes. Pair potentials were derived using the SS and MS IBI methods, using the results of the UA simulations as target data, as discussed in detail in Section III. The bond stretching and angle bending potentials used in the study of dodecane were derived by a Boltzmann inversion of the bonded distributions sampled in the atomistic trajectory mapped to the CG level.[53] Specifically, from a normalized bond length distribution $p(r)$, the bond stretching potential is written as

$$V_{bond}(r) = -k_B T \ln p(r) \quad (5)$$

which, assuming a Gaussian bond length distribution, results in a harmonic potential about the most probable bond length, r_{eq} ; note an identical formalism was used for angles, where θ is substituted for r , and the normalization includes a factor of $\sin^{-1} \theta$. Since minimal state dependence was found between systems, a single set of bonded parameters was used in all simulations, with $k/k_B = 15.60 \text{ K}/\text{\AA}$ and $r_{eq} = 3.56 \text{ \AA}$ for bonds and $k/k_B = 0.17 \text{ K/deg}^2$ and $\theta_{eq} = 174.53 \text{ \AA}$ for angles. Bond histograms and additional details are included in the Supplemental Material.[56]

In all cases, the GPU-enabled HOOMD-Blue[57]·[58] simulation engine was used to perform the simulations. The high performance of the GPU allows for rapid derivation of potentials. A standard potential optimization using MS IBI required approximately 50 iterations to be well-converged. For the pure LJ systems with 1468 particles, this convergence took less than one hour using three NVidia GTX580 GPUs concurrently. The following convergence criteria was used to measure how well a trial RDF matched with its target, where dr is the size of an RDF bin:

$$f_{fit} = 1 - \frac{\int_0^{r_{cut}} dr |g^i(r) - g^*(r)|}{\int_0^{r_{cut}} dr |g^i(r) + g^*(r)|} \quad (6)$$

An f_{fit} value of unity represents a perfect match between the trial and target RDFs. Additionally, in all figures, the following two-point central moving average smoothing function was applied to the derived potential to reduce the noise:

$$V'_n(r) = \frac{1}{3} [V_{n-1}(r) + V_n(r) + V_{n+1}(r)] \quad (7)$$

where $V_n(r)$ is the n^{th} element of the numerical potential, and the prime denotes the smoothed value. The application of the smoothing function was not found to significantly influence the behavior or degree of matching.

III. RESULTS

A. Monatomic Lennard-Jones fluid

To test the efficacy of the MS IBI method, potentials were derived using RDFs from monatomic LJ spheres as target data, and the results compared to single state potential derivation (i.e., SS IBI). Target data was acquired from the following states: state A, reduced density $\rho^* = N\sigma^3/V = 0.85$, reduced temperature $T^* = k_B T/\epsilon = 0.5$; state B, $\rho^* = 0.67$, $T^* = 1.5$; and state C, $\rho^* = 0.18$, $T^* = 2.0$. No coarse-graining was performed since the goal was to test whether the MS IBI method could recover a known potential. In contrast to mapping an atomistic system to the CG level, no information about the system is lost ensuring that a single potential is applicable to all states and that this potential is known.

While the RDFs match well, as illustrated in Figure 2, the potentials derived via SS IBI demonstrate significant state dependence, as shown in Figure 2d. For the more dense states A and B (Figures 2a,b), the SS IBI method was not able to converge to the true potential to the extent that in the most dense system (state A), the converged potential is almost purely repulsive. This result is due to the elevated density of this state, where the structure can be reproduced with a purely repulsive potential.[59] In this case, even though the RDF matches the target well, the overall behavior of the system would be dramatically altered as compared to the target. A similar situation arises in state B where only a weak attractive potential is required to match the target structure. In state C, however, the low density causes attractive forces to become important, and as such, the attractive portion of the LJ potential is needed to fully reproduce the target data. Thus, the true LJ potential is recovered only for state C. The application of SS IBI to the monatomic LJ system illustrates two points: (1) that potentials derived via SS IBI are state-dependent, and (2) these potentials are not unique, in that both the LJ potential and the vastly differing derived potential produce matching RDFs.

MS IBI aims to address the aforementioned issues by forcing the potential to sample portions of potential phase space that satisfy all of the constraints, i.e., find a single potential that matches the target structure at multiple states. The results of applying MS IBI to the monatomic LJ fluid are shown in Figure 2e-h. The inclusion of target data from multiple states results in closely matching RDFs and a derived potential that accurately reproduces the true LJ potential, as shown in Figure 2h. Although this example is simple, as no coarse-graining was performed, it illustrates the ability of MS IBI to recover a known potential and reduce the state-dependence of the derived potential.

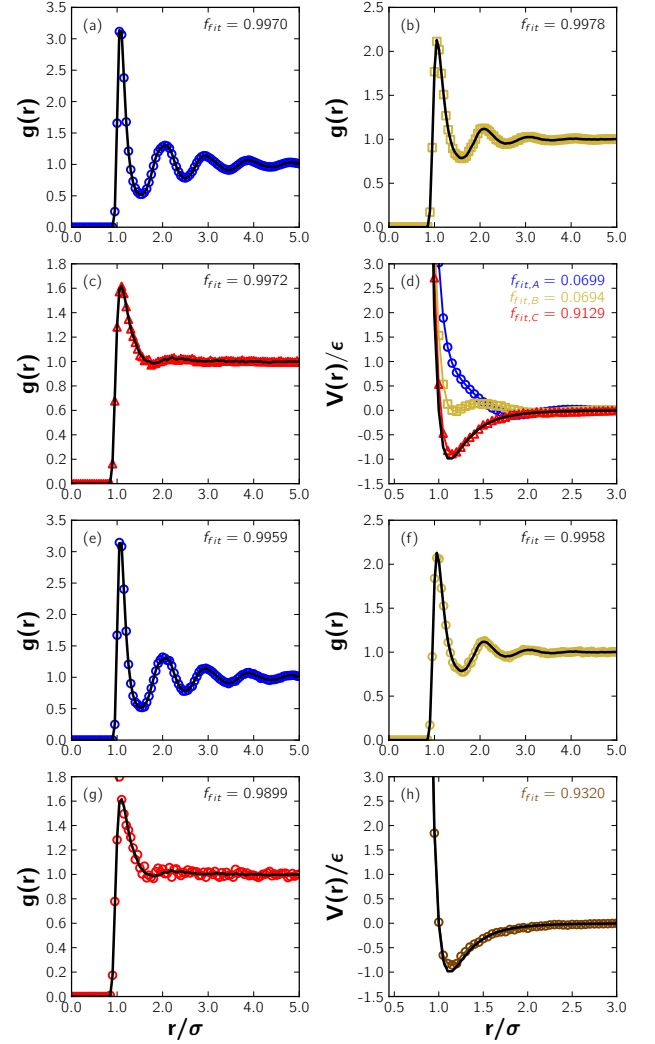


FIG. 2. RDFs and potentials derived for the LJ system. (a-d) SS IBI results. (e-h) MS IBI results. The α value used for the MS IBI optimizations was 0.7 for each state. f_{fit} for the potentials was calculated in the range $\sigma \leq r \leq r_{cutoff}$. The solid black line represents the target RDF (a-c, e-g) or the known potential (d, h). The symbols represent the derived potential (d, h) or the RDFs calculated from simulations using the derived potential (a-c, e-g).

B. Propane

To further test the MS IBI algorithm, potential optimizations were performed on propane. The chosen 3-to-1 mapping results in a single-site model that can be directly compared to known single site 12-6 LJ models from the literature.[60] Note, the 12-6 LJ potential should not be considered to be the “true” potential, but rather a good approximation. Target data was acquired from UA simulations at the following states: state A, 298 K, 0.818 g/mL, $\alpha_A(0) = 0.5$; state B, 298 K, 0.439 g/mL, $\alpha_B(0) = 0.7$, and state C, 298 K, 0.014 g/mL,

$\alpha_C(0) = 0.5$. The resulting RDFs and (single) pair potential are presented in Figure 3. At each state, f_{fit} indicates excellent agreement between the target RDFs and those calculated from simulations using the derived potential. Moreover, we find that the derived potential agrees well with a single-site 12-6 LJ model using parameters mapped to the critical point of propane,[60] providing confidence in the MS IBI method. While the match between the two potentials is good, the derived potential does show two small bumps at ~ 7 Å and another at ~ 9.5 Å, which are likely related to orientational effects; that is, likely related to treating the three UA carbon groups as a single, spherically symmetric interaction site.

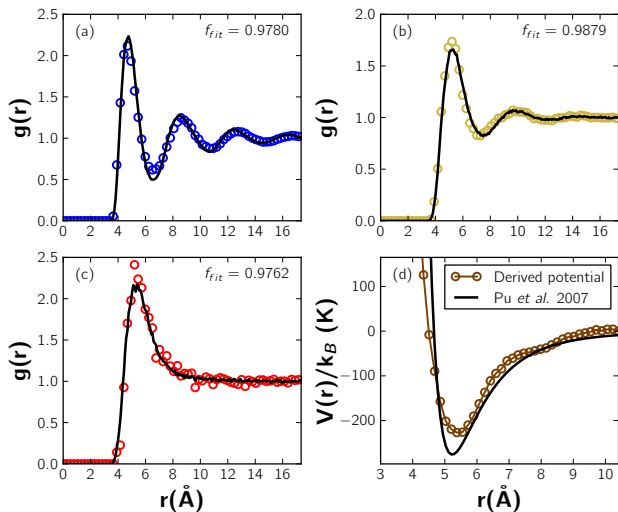


FIG. 3. RDFs (a-c) and potential (d) derived for propane using MS IBI. a, b, and c correspond to states A, B, and C in the text, respectively. The α values used were 0.5, 0.7, and 0.5 for states A, B, and C, respectively.

To illustrate the consistency of the potentials derived via MS IBI (i.e., that the final potential is insensitive to the initial guess), optimizations were performed using a number of different initial potentials. In addition to the PMF-like quantity of Equation 3, three additional initial guesses were used, each a 12-6 LJ potential with vastly differing parameters: (1) $\varepsilon_1 = 0.46$ kcal/mol, $\sigma_1 = 4.51$ Å; (2) $\varepsilon_2 = 0.001$ kcal/mol, $\sigma_2 = \sigma_1$; (3) $\varepsilon_3 = 2\varepsilon_1$, $\sigma_3 = \sigma_1$; The final derived potentials are, in each case, very similar to each other and to the derived potential in Figure 3d, as shown in Figure 4. Particularly, the f_{fit} values between each potential and the derived potential shown in Figure 3 are 0.986, 0.980, and 0.986, respectively.

C. *n*-dodecane

To look at a more complex system and test the state-independence, we look at *n*-dodecane in the bulk and use it to examine systems containing monolayers. Inter-

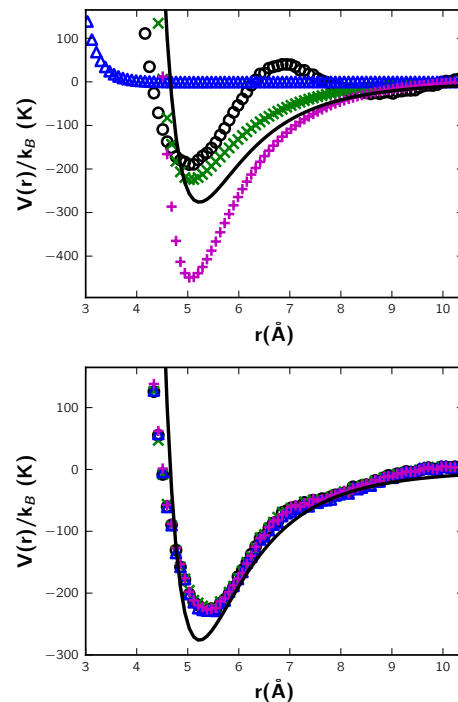


FIG. 4. Different initial guesses (top) and the resulting derived potentials (bottom) for propane optimizations. Blue triangles: LJ with $\varepsilon = \varepsilon_2$ and $\sigma = \sigma_2$; black circles: $V_0(r)$ from Eq. 3 (same as shown in Figure 3); green 'x': LJ with $\varepsilon = \varepsilon_1$ and $\sigma = \sigma_1$; solid black line: 1-site propane model[60] (not used as initial guess, shown for reference); magenta '+': LJ with $\varepsilon = \varepsilon_3$ and $\sigma = \sigma_3$. Symbols in top plot correspond to the same symbols in the bottom plot. Note that all potentials converge to very similar values.

molecular pair potentials were derived for the beads of a CG model of *n*-dodecane, again using a 3-to-1 mapping. The resulting 4-site model contains two middle beads and two terminal beads, where middle and terminal beads were treated as unique entities, resulting in the need to derive three pair potentials; harmonic bonds and angles were used, as detailed in the methods section. The target data was collected from UA simulations of *n*-dodecane at the following states: state A, 298 K, 1.04 g/mL; state B, 298 K, 0.74 g/mL; and state C, 370 K, 0.55 g/mL; the damping values used were $\alpha_A(0) = 0.5$, $\alpha_B(0) = 0.7$, and $\alpha_C(0) = 0.5$. Note that state B corresponds to the experimental density at standard ambient temperature and pressure, and, as such, is given higher weight than the other states in this example. Close agreement with the target RDFs is found, with an f_{fit} value greater than 0.98 for each of the nine RDFs calculated (not shown, see Supplemental Material). To further assess the quality of the potentials derived via MS IBI, the average squared radius of gyration normalized by the average end-to-end distance, denoted by R_{chain} , was calculated, providing a measure of the chain conformations at different thermodynamic states. Using potentials derived with MS IBI,

good agreement is seen between the UA target data and the CG model of the ratio R_{chain} , as shown in Figure 5; in this plotting scheme an ideal match corresponds to a data point situated on the line $y = x$. While deviations become more apparent as R_{chain} increases, the potentials derived from only state B (i.e., standard temperature and pressure) via SS IBI show larger, systematic deviations of R_{chain} over the entire range of state points considered. As such, it appears the potential from MS IBI more accurately models the conformations of dodecane over a range of state points. Note, in both cases, additional simulations were performed at state points not used in the fitting (state points used in the fitting are highlighted with open squares in Figure 5), to also test the transferability of the derived potential. The improved match of chain conformations was further tested by examining systems containing n -dodecane monolayers.

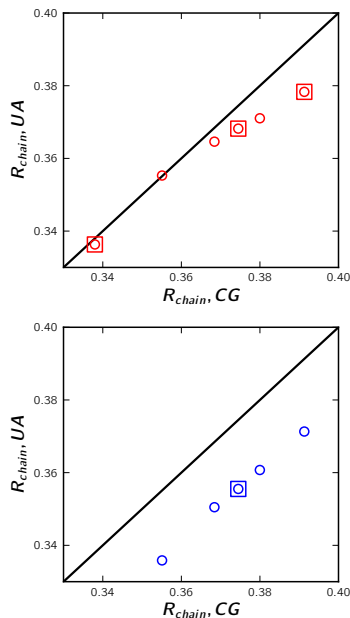


FIG. 5. Comparison of a structural metric between the CG and UA models of n -dodecane. The CG potentials were derived from MS IBI (top) and SS IBI (bottom). A value lying on the solid line represents a perfect match between the CG and UA models. Squares represent data points from simulations at state points where the potential was derived; circles are data points from other states used for testing the state dependence. The states used in the multi-state fitting are states A, B, and C as described above with $\alpha_A(0) = 0.5$, $\alpha_B(0) = 0.7$, and $\alpha_C(0) = 0.5$. State B was used for the single state fitting with $\alpha = 0.7$.

D. n -dodecane Monolayer

As mentioned in Section II B, here the damping coefficient, $\alpha_s(r)$, is a function of both separation, r , and state, s . Recall that the dependence on separation is cho-

sen such that the derived potential has a value of zero at the potential cutoff as well as to reduce the influence of intermediate and long-range structural correlations on the derived potentials. Adjusting the $\alpha_s(0)$ value given to each state effectively alters the weight given to each state in the fitting, i.e., more or less emphasis can be placed on a given state. While adjusting the relative weight given to each state may have only a small effect on the derived RDFs, it may alter the potential, which ultimately may vary other system properties, allowing potentials to be tuned to capture specific behaviors. To demonstrate this, as well as to further test the transferability of the derived potentials, alkane monolayers were simulated with the 3-to-1 CG model, with potentials optimized in the bulk states discussed above, using various values of $\alpha_s(0)$ for each of the three states. The average tilt angle, θ , with respect to the surface and the nematic order parameter, S_2 , of the chains were calculated[61] and compared with those values calculated from the corresponding UA simulations. Note that the UA monolayer simulations were not used as target data in the potential derivation, used only to validate the properties predicted by the derived CG potential.

Unique sets of CG potentials were derived over a range of $\alpha_s(0)$ values, as summarized in Table I. Here, the states A, B, and C are the same states previously used as target data to derive a CG potential for bulk systems of n -dodecane above. The results indicate that both the average chain tilt angle and the nematic order parameter are functions of the relative $\alpha_s(0)$ weights for the fluid state monolayer. For the gel phase monolayer, the nematic order parameter is less dependent on the $\alpha_s(0)$ values, while the chain tilt angle is significantly dependent.

Initially, potentials were optimized with equal weights assigned to each state. As shown in Table I, this α set yields a potential that significantly overpredicts the fluid phase order parameter, while it underpredicts the gel phase chain tilt. Since the monolayers are inherently somewhat ordered, it would be expected that increasing the relative weight given to the most dense state, state A, would yield a potential that better captures the system behavior. By systematically reducing the weight given to the less dense states, first state C, then state B, a potential that very closely reproduces the monolayer behavior is obtained for α values of 0.7, 0.1, and 0.1 for state A, B, and C, respectively. Given the small weights assigned to states B and C in this case, it may be expected that this potential would give results similar to the potential derived via SS IBI at state A. However, it can be seen in Table I that this clearly is not the case; potentials derived from SS IBI at state A show large deviations, underpredicting both the average tilt angle and nematic order parameter in the gel phase monolayer, in stark contrast to the near perfect behavior predicted by MS IBI. This result is a direct consequence of using the MS IBI method; even though low weights are given to the other states, the derived potentials will only be consid-

ered converged if all states demonstrate good agreement. Again, we note that when deriving the potentials, the UA monolayer was not used as target data (i.e., the structure matching was performed in the same manner as described in Section III C, except with varying values of $\alpha_s(0)$ for each state). The close match that is observed is a result of the success of the MS IBI method in deriving a more generally applicable, transferable, set of potentials.

IV. CONCLUSION

A multistate extension of the popular IBI method has been proposed. In the proposed MS IBI method, multiple thermodynamic states are used in the derivation of a single, generally applicable potential. For systems with a known potential, it was shown that the MS IBI method was capable of accurately recovering the true, underlying potential, while the SS IBI method was unable to consistently derive a generally applicable potential. Through the coarse-graining of propane, it was shown that MS IBI was able to recover a potential very similar to a previously published single-site model with good reproducibility. Furthermore, potentials derived via MS IBI were shown to better reproduce structural conformations of *n*-dodecane than potentials derived via SS IBI. It was also demonstrated that adjusting the relative weights given to each target in the optimizations can be used to tune system properties beyond the RDF; in this case, tuning the weights enabled potentials to be derived that provided near perfect agreement between CG and atomistic models when considering the nematic order parameter and tilt angle of an *n*-dodecane monolayer. While pressure, and thermodynamics in general, were not investigated in this work, the standard pressure correction scheme of SS IBI[38] could be trivially applied to MS IBI by calculating the average pressure deviations between all states, and using this quantity in the pressure correction term.

As such, the MS IBI stands as an improvement of the typical IBI method, producing more generally applicable potentials that can be tuned to match target properties from experiment or finer-grained simulations.

This improved methodology should be very useful for a host of molecular systems, including, for example, lipid systems, where not only do systems demonstrate structural heterogeneity within a given state point (i.e., different molecular structures in a single system), but properties such as tilt angle, nematic order, area per lipid, etc., need to be tuned in order to match atomistic simulations and experiment. [62–66] Given that the MS IBI approach is also capable of deriving potentials which demonstrate increased levels of transferability than SS IBI, potentials can be derived for complex systems with many unique interactions by examining the individual components separately, reducing the number of simultaneous optimizations that need to be performed. Furthermore, this work presents a method to develop potentials that enable the examination of phase transitions; in many prior works utilizing SS IBI, different potentials are needed to appropriately model different states, making it difficult to accurately examine the transition between those states. [18, 45, 67, 68] Additionally, given that multi-GPU machines and GPU enabled simulation packages[57, 69–72] are becoming more common, the potential derivation process can be carried out with relatively little computational effort, even if a large number of targets are needed, or a large number of iterations must be undertaken to find appropriate weighting functions.

ACKNOWLEDGMENTS

The authors acknowledge support from grant number R01 AR057886-01 from the National Institute of Arthritis and Musculoskeletal and Skin Diseases.

-
- [1] J. N. Israelachvili, D. J. Mitchell, and B. W. Ninham, *J. Chem. Soc., Faraday Trans. 2* **72**, 1525 (1976).
 - [2] J. N. Israelachvili, D. J. Mitchell, and B. W. Ninham, *Biochimica et Biophysica Acta (BBA)-Biomembranes* **470**, 185 (1977).
 - [3] I. Mušević and M. Škarabot, *Soft Matter* **4**, 195 (2008).
 - [4] K. J. Bishop, C. E. Wilmer, S. Soh, and B. A. Grzybowski, *small* **5**, 1600 (2009).
 - [5] C. R. Iacovella, A. S. Keys, and S. C. Glotzer, *Proc. of the Nat. Ac. of Sci.* **108**, 20935 (2011).
 - [6] P. Ziherl and R. D. Kamien, *J. Phys. Chem. B* **105**, 10147 (2001).
 - [7] E. L. Thomas, D. J. Kinning, D. B. Alward, and C. S. Henkee, *Macromol.* **20**, 2934 (1987).
 - [8] C. L. Phillips, C. R. Iacovella, and S. C. Glotzer, *Soft Matter* **6**, 1693 (2010).
 - [9] C. R. Iacovella and S. C. Glotzer, *Nano Lett.* **9**, 1206 (2009).
 - [10] M. A. Glaser, G. M. Grason, R. D. Kamien, A. Košmrlj, C. D. Santangelo, and P. Ziherl, *Europhys. Lett.* **78**, 46004 (2007).
 - [11] P. Ziherl and R. D. Kamien, *Phys. Rev. Lett.* **85**, 3528 (2000).
 - [12] R. Larson, L. Scriven, and H. Davis, *J. Chem. Phys.* **83**, 2411 (1985).
 - [13] S. C. Glotzer, M. A. Horsch, C. R. Iacovella, Z. Zhang, E. R. Chan, and X. Zhang, *Current Opinion in Colloid & Interface Science* **10**, 287 (2005).
 - [14] L. Gai, K. A. Maerzke, P. T. Cummings, and C. McCabe, *J. Chem. Phys.* **137**, 144901 (2012).
 - [15] C. R. Iacovella, M. A. Horsch, Z. Zhang, and S. C. Glotzer, *Langmuir* **21**, 9488 (2005).
 - [16] K. F. Lau and K. A. Dill, *Macromol.* **22**, 3986 (1989).
 - [17] K. A. Maerzke and J. I. Siepmann, *J. Phys. Chem. B* **115**, 3452 (2011).
 - [18] S. J. Marrink, H. J. Risselada, S. Yefimov, D. P. Tiele-

TABLE I. Average chain tilt with respect to surface normal, θ , and nematic order parameter, S_2 , for the monolayers in the fluid state (subscript F) and in the gel state (subscript G). The states A, B, and C are the same ones used in Section III C. Values are given as ensemble averages \pm standard deviation.

$\alpha_A / \alpha_B / \alpha_C$	θ_F	$S_{2,F}$	θ_G	$S_{2,G}$
0.7/0.7/0.7	$19 \pm 6.3^\circ$	0.97 ± 0.013	$18 \pm 6.5^\circ$	0.98 ± 0.017
0.7/0.7/0.6	$20 \pm 6.1^\circ$	0.97 ± 0.012	$20 \pm 3.7^\circ$	0.992 ± 0.0018
0.7/0.7/0.5	$18 \pm 6.9^\circ$	0.96 ± 0.020	$20 \pm 3.8^\circ$	0.991 ± 0.0022
0.7/0.7/0.4	$15 \pm 7.0^\circ$	0.95 ± 0.018	$20 \pm 4.0^\circ$	0.990 ± 0.0027
0.7/0.7/0.3	$13 \pm 6.8^\circ$	0.94 ± 0.019	$19 \pm 4.2^\circ$	0.990 ± 0.0036
0.7/0.7/0.2	$12 \pm 6.3^\circ$	0.93 ± 0.014	$12 \pm 6.4^\circ$	0.96 ± 0.014
0.7/0.7/0.1	$10 \pm 5.6^\circ$	0.95 ± 0.011	$8 \pm 5.3^\circ$	0.958 ± 0.008
0.7/0.4/0.1	$18 \pm 9.0^\circ$	0.83 ± 0.021	$29 \pm 3.9^\circ$	0.988 ± 0.0026
0.7/0.1/0.1	$20 \pm 10^\circ$	0.81 ± 0.023	$32.2 \pm 3.6^\circ$	0.989 ± 0.002
SS IBI, state A	$17 \pm 8.8^\circ$	0.85 ± 0.017	$15 \pm 7.4^\circ$	0.89 ± 0.014
SS IBI, state B	$23 \pm 4.9^\circ$	0.983 ± 0.005	$21.3 \pm 3.3^\circ$	0.993 ± 0.001
SS IBI, state C	$23 \pm 4.1^\circ$	0.988 ± 0.002	$20 \pm 4.6^\circ$	0.987 ± 0.002
United Atom	$20 \pm 15^\circ$	0.820 ± 0.028	$32.4 \pm 10.1^\circ$	0.965 ± 0.046

- man, and A. H. de Vries, J. Phys. Chem. B **111**, 7812 (2007).
- [19] M. G. Martin and J. I. Siepmann, J. Phys. Chem. B **102**, 2569 (1998).
- [20] W. L. Jorgensen, D. S. Maxwell, and J. Tirado-Rives, J. Am. Chem. Soc. **118**, 11225 (1996).
- [21] C. Oostenbrink, A. Villa, A. E. Mark, and W. F. Van Gunsteren, J. Comp. Chem. **25**, 1656 (2004).
- [22] K. Vanommeslaeghe, E. Hatcher, C. Acharya, S. Kundu, S. Zhong, J. Shim, E. Darian, O. Guvench, P. Lopes, I. Vorobyov, *et al.*, J. Comp. Chem. **31**, 671 (2010).
- [23] J. Wang, R. M. Wolf, J. W. Caldwell, P. A. Kollman, and D. A. Case, J. Comp. Chem. **25**, 1157 (2004).
- [24] C. McCabe, S. C. Glotzer, J. Kieffer, M. Neurock, and P. T. Cummings, J. Comp. and Theor. Nanosci. **1**, 265 (2004).
- [25] H. Liu, M. Li, Z.-Y. Lu, Z.-G. Zhang, C.-C. Sun, and T. Cui, Macromol. **44**, 8650 (2011).
- [26] C. Peter and K. Kremer, Soft Matter **5**, 4357 (2009).
- [27] N. Di Pasquale, D. Marchisio, and P. Carbone, J. Chem. Phys. **137**, 164111 (2012).
- [28] B. Ensing, S. O. Nielsen, P. B. Moore, M. L. Klein, and M. Parrinello, J. Chem. Theory and Comp. **3**, 1100 (2007).
- [29] E. Lidorikis, M. E. Bachlechner, R. K. Kalia, A. Nakano, P. Vashishta, and G. Z. Voyiadjis, Phys. Rev. Lett. **87**, 086104 (2001).
- [30] J. Michel, M. Orsi, and J. W. Essex, J. Phys. Chem. B **112**, 657 (2008).
- [31] M. Praprotnik, L. D. Site, and K. Kremer, Annu. Rev. Phys. Chem. **59**, 545 (2008).
- [32] A. J. Rzepiela, M. Louhivuori, C. Peter, and S. J. Marrink, Phys. Chem. Chem. Phys. **13**, 10437 (2011).
- [33] T. Werder, J. H. Walther, and P. Koumoutsakos, J. Comp. Phys. **205**, 373 (2005).
- [34] A. P. Heath, L. E. Kaviraki, and C. Clementi, Proteins: Structure, Function, and Bioinformatics **68**, 646 (2007).
- [35] B. Hess, C. Holm, and N. van der Vegt, J. Chem. Phys. **124**, 164509 (2006).
- [36] P. Liu, Q. Shi, E. Lyman, and G. A. Voth, J. Chem. Phys. **129**, 114103 (2008).
- [37] A. J. Rzepiela, L. V. Schäfer, N. Goga, H. J. Risselada, A. H. De Vries, and S. J. Marrink, J. Comp. Chem. **31**, 1333 (2010).
- [38] D. Reith, M. Pütz, and F. Müller-Plathe, J. Comp. Chem. **24**, 1624 (2003).
- [39] F. Ercolessi and J. B. Adams, Europhys. Lett. **26**, 583 (1994).
- [40] S. Izvekov and G. A. Voth, J. Phys. Chem. B **109**, 2469 (2005).
- [41] M. S. Shell, J. Chem. Phys. **129**, 108 (2008).
- [42] A. Chaimovich and M. S. Shell, J. Chem. Phys. **134**, 094112 (2011).
- [43] C. R. Iacovella, R. E. Rogers, S. C. Glotzer, and M. J. Solomon, J. Chem. Phys. **133**, 164903 (2010).
- [44] B. Bozorgui, D. Meng, S. K. Kumar, C. Chakravarty, and A. Cacciuto, Nano Lett. **13**, 2732 (2013).
- [45] K. Hadley and C. McCabe, J. Chem. Phys. **132**, 134505 (2010).
- [46] R. Faller, Polymer **45**, 3869 (2004).
- [47] C.-C. Fu, P. M. Kulkarni, M. S. Shell, and L. G. Leal, J. Chem. Phys. **137**, 164106 (2012).
- [48] H.-J. Qian, P. Carbone, X. Chen, H. A. Karimi-Varzaneh, C. C. Liew, and F. Muller-Plathe, Macromol. **41**, 9919 (2008).
- [49] B. Bayramoglu and R. Faller, Macromol. **45**, 9205 (2012).
- [50] B. Bayramoglu and R. Faller, Macromol. **46**, 7957 (2013).
- [51] P. Ganguly and N. F. van der Vegt, J. Chem. Theory and Comp. **9**, 1347 (2013).
- [52] E. R. Chan, A. Striolo, C. McCabe, P. T. Cummings, and S. C. Glotzer, J. Chem. Phys. **127**, 114102 (2007).
- [53] G. Milano, S. Goudeau, and F. Müller-Plathe, J. of Polymer Science Part B: Polymer Phys. **43**, 871 (2005).
- [54] K. Hadley and C. McCabe, Biophys. J. **99**, 2896 (2010).
- [55] J. L. Rivera, G. K. Jennings, and C. McCabe, J. Chem. Phys. **136**, 244701 (2012).
- [56] See supplemental material at [URL will be inserted by AIP] for derivation of *n*-dodecane pair and bonded potentials and associated RDFs.
- [57] J. A. Anderson, C. D. Lorenz, and A. Travesset, J. Comp. Phys. **227**, 5342 (2008).
- [58] <http://codeblue.umich.edu/hoomd-blue>.
- [59] J. D. Weeks, D. Chandler, and H. C. Andersen, J. Chem. Phys. **54**, 5237 (1971).
- [60] Q. Pu, Y. Leng, X. Zhao, and P. T. Cummings, Nanotech. **18**, 424007 (2007).

- [61] A. S. Keys, C. R. Iacovella, and S. C. Glotzer, *J. Comp. Phys.* **230**, 6438 (2011).
- [62] H. Heller, M. Schaefer, and K. Schulten, *J. Phys. Chem.* **97**, 8343 (1993).
- [63] E. Egberts, S.-J. Marrink, and H. J. Berendsen, *Euro. Biophys. J.* **22**, 423 (1994).
- [64] L. Saiz and M. L. Klein, *Accounts of Chemical Research* **35**, 482 (2002).
- [65] H. L. Scott, *Current Opinion in Structural Biology* **12**, 495 (2002).
- [66] M. Venturoli, M. Maddalena Sperotto, M. Kranenburg, and B. Smit, *Physics Reports* **437**, 1 (2006).
- [67] T. Vettorel and H. Meyer, *J. Chem. Theory and Comp.* **2**, 616 (2006).
- [68] G. D’Adamo, A. Pelissetto, and C. Pierleoni, *Soft Matter* **8**, 5151 (2012).
- [69] B. Hess, C. Kutzner, D. Van Der Spoel, and E. Lindahl, *J. Chem. Theory and Comp.* **4**, 435 (2008).
- [70] S. Plimpton, *J. Comp. Phys.* **117**, 1 (1995).
- [71] W. M. Brown, P. Wang, S. J. Plimpton, and A. N. Tharrington, *Computer Phys. Comm.* **182**, 898 (2011).
- [72] W. M. Brown, A. Kohlmeier, S. J. Plimpton, and A. N. Tharrington, *Computer Phys. Comm.* **183**, 449 (2012).